Computational Geosciences (2024) 28:195–210
https://doi.org/10.1007/s10596-023-10213-6

ORIGINAL PAPER

Multi-objective optimization of subsurface CO_2 capture, utilization, and storage using sequential quadratic programming with stochastic gradients

Quang Minh Nguyen[1] · Mustafa Onur[1] · Faruk Omer Alpak[2]

Received: 14 November 2022 / Accepted: 20 April 2023 / Published online: 17 June 2023

Abstract
Carbon capture, utilization, and storage (CCUS) is a crucial part of the energy industry nowadays, aiming to reduce the overall carbon emission into the environment. One solution to CCUS is via the means of CO_2 enhanced recovery processes in a depleted oil reservoir. In such a case, life-cycle production optimization plays a crucial component, referring to optimizing a production-driven objective function via varying well controls during a reservoir's lifetime. One challenge is to obtain the optimal cash flow while trying to maintain the maximum CO_2 storage. Another challenge is the nonlinear constraints (such as field liquid production rate) which need to be honored due to the capacity of the processing facilities. This study presents an application of a stochastic gradient-based framework to solve the CO_2 storage multi-objective optimization problem. Our study focuses on carbon capture and storage via the means of nonlinearly constrained production optimization workflow for a CO_2 enhanced recovery process, in which we aim to bi-objectively maximize both the net-present-value (NPV) and the net present carbon tax credits (NPCTC). The main framework used in this work is line-search sequential quadratic programming (LS-SQP) with stochastic simplex approximated gradients (StoSAG). We demonstrate the performance and results of the algorithmic framework in a field-scale realistic problem. The case study being investigated is a multiphase flow Brugge model under CO_2 injection, simulated using a commercial compositional reservoir simulator. Results show that the LS-SQP algorithm with StoSAG gradients performs computationally efficiently and effectively in handling nonlinear state constraints imposed onto the problem. The workflow successfully solves both the single-objective and the multi-objective optimization problems with minimal and acceptable constraint violations. Various numerical settings have been experimented with to estimate the Pareto front for the bi-objective optimization problem, showing the trade-off between the two objectives NPV and NPCTC. We have demonstrated an approach to the carbon capture, utilization, and storage (CCUS) in the context of multi-objective production optimization of a CO_2 enhanced recovery process for a field-scale realistic reservoir model. The algorithmic framework used in this study has proven to be computationally effective on the problem and especially useful when utilized in conjunction with commercial flow simulators that lack the capability of computing adjoint-based gradients.

Keywords Multi-objective optimization · CCUS · Well control optimization · Pareto front · Sequential quadratic programming · Stochastic simplex approximate gradient · Brugge model · Reservoir simulation

1 Introduction

Large-scale deployment of carbon dioxide (CO_2) capture, utilization, and storage (CCUS) technologies is a critical enabler for the transition to a decarbonized economy. Thus, CCUS has become a crucial part of the energy industry nowadays, aiming to reduce the overall carbon emission into the environment. In subsurface engineering applications, CCUS processes could be conducted through geological carbon storage (or sequestration) technology. This involves the substantial elimination of CO_2 from the Earth's atmosphere and permanent storage by injection into deep underground geological formations with structural closure, such as saline aquifers or depleted oil/gas reservoirs. Other than the permanent geological carbon sequestration, another solution

✉ Quang Minh Nguyen
qun972@utulsa.edu

[1] Petroleum Engineering Department, The University of Tulsa, Tulsa, OK 74104, USA

[2] Shell International Exploration and Production Inc, Shell Technology Center Houston, Houston, TX 77082, USA

to CCUS is via the means of CO_2 enhanced oil recovery (EOR) processes. Not only these processes could safely sequester some of the CO_2 from the atmosphere in some certain degrees, but also allow additional hydrocarbons to be recovered and marketed, resulting in more profit to be earned.

During the design phase of a CO_2-EOR process with specified well placement, coming up with a set of optimal well controls is important. In such a case, life-cycle production optimization plays a crucial component, referring to optimizing (maximizing or minimizing) a production-driven objective function via altering well controls during a reservoir's lifetime [7, 10, 22]. One challenge arisen is to obtain the optimal cash flow while also trying to maintain the maximum CO_2 storage, which could be either in terms of quantity such as mass or volume, or in terms of carbon tax credits [23]. This concern in the decision making process is one of the situations where we have conflicting criteria or objectives, hence a multi-objective optimization solution [2, 3, 41] needs to be considered. Another challenge in the project design is the nonlinear state constraints due to the capacity of the processing facilities [1, 5, 25, 29, 30, 34], which need to be honored as parts of the life-cycle production optimization process. Therefore, it is necessary to have a computationally effective and efficient algorithmic framework to handle these nonlinearly constrained multi-objective optimization problems.

There exists many algorithms to solve a multi-objective optimization problem, and they generally could be classified as derivative-free and gradient-based. The derivative-free algorithms such as genetic algorithms [20] or particle swarm optimization algorithms [6] are capable of avoiding or escaping from the local minima, however, the computational cost of these methods could easily become infeasible as the dimension of the design variable vector exceeds a hundred, and/or if the evaluation of the objective function requires running a complex numerical model. Isebor and Durlofsky [21] presented a derivative-free strategy to solve a bi-objective optimization problem. However, their method required on the order of 800,000 simulation runs to generate the bi-objective Pareto front, which would be impractical for realistic optimization problems. Thus, for large-scale problems, gradient-based methods are much more computationally efficient, especially when the derivative information is available. The Augmented Lagrangian method (ALM) has been traditionally known as an external penalty method to handle nonlinear optimization problems [35]. However, the biggest drawback of ALM is its computational cost since the process involves both outer-loop and inner-loop procedures, especially in the specific context of production optimization [9, 12, 31] in which reservoir simulations are needed to evaluate the objective function value repetitively, making the method particularly computationally demanding. Liu et al. [28] demonstrated that sequential quadratic programming (SQP) methods significantly outperform ALM, both in terms of computational cost and the ability to handle nonlinear constraints, thus making SQP a better and more suitable alternative than ALM for nonlinear optimization problems.

Various methods are available to solve multi-objective optimization problems. Popular ones such as the weighted sum (WS) method [19, 43], the normal boundary intersection (NBI) method [15], and the lexicographic method [32] can be implemented via the use of the gradient information. A common feature of these three methods is that they all transform the original multi-objective optimization problem into one or a series of single-objective optimization problems. Liu and Reynolds [26] utilized the constrained WS and constrained NBI methods to solve the bi-objective production optimization problem, with the presence of the nonlinear constraints using ALM. In the work of [27], they also applied the lexicographic method to solve the bound-constrained bi-objective production optimization problem. The work presented in both [26] and [27] is limited to adjoint gradient solutions. To the best of our knowledge, when dealing with commercial and proprietary reservoir simulators, typically they either have very limited or no adjoint capability at all, with the exception of the one described in [24]. Due to this reason, stochastic gradients are considered as the best alternative approach instead [8, 18, 30], as they allow the users to treat the reservoir simulator as a black box.

Recently, [34] have developed an efficient line-search sequential quadratic programming (LS-SQP) algorithmic framework coupled with stochastic simplex approximated gradients (StoSAG) by [18] to handle nonlinearly constrained production optimization problems. In that paper, we compared the performances of ALM, LS-SQP, and trust-region SQP (TR-SQP) for nonlinearly constrained robust optimization problems with StoSAG gradients. The results indicate the superiority of SQP over ALM, which is consistent with the conclusions by [28], but with stochastic gradients. Therefore, in this article, we are applying the LS-SQP workflow [34] to our study focusing on CCUS in the context of nonlinearly constrained multi-objective deterministic production optimization workflow for a CO_2-EOR process, in which we aim to bi-objectively maximize both the net present value (NPV) and the net present carbon tax credit (NPCTC).

This paper is organized as follows. Firstly, we present the theory and methodology. Then, we present the results with a benchmark example for the Brugge field, which is a synthetic field originally used for closed-loop reservoir management [11, 13, 16, 37]. The specific case study being investigated is a compositional multiphase flow Brugge model under CO_2 injection, simulated using a commercial compositional reservoir simulator. We demonstrate the performance of the workflow in solving the bi-objective optimization problem using the lexicographic method with minimal constraint violations. Additionally, we also experimented with various numerical settings to approximate the Pareto front for the

bi-objective problem, showing the trade-off between the two competing objectives of NPV and NPCTC.

2 Theory and methodology

In this section, we describe the theory and methodology used to perform bi-objective optimization of CO_2 storage by SQP based on StoSAG method.

2.1 Constrained multi-objective production optimization problem

The typical single-objective deterministic production optimization problem refers to the estimation of the optimal design variables on predefined control time steps which minimize the negative net present value (NPV), or equivalently, maximizing the NPV of life-cycle production. The optimization problem is subject to bound constraints and operational constraints which are typically represented as nonlinear state constraints. For a three-phase flow deterministic reservoir under CO_2 injection, the negative life-cycle NPV function is defined as

$$J_{\mathrm{NPV}}(\mathbf{u}) = -\sum_{n=1}^{N_t} \frac{\Delta t_n}{(1+b)^{\frac{t_n}{365}}} \times \left\{ \sum_{i=1}^{N_\mathrm{P}} \left(c_o \cdot \overline{q}^n_{o,i} - c_w \cdot \overline{q}^n_{w,i} - c_{\mathrm{CO_2\text{-}prd}} \cdot \overline{q}^n_{\mathrm{CO_2\text{-}prd},i} \right) - \sum_{j=1}^{N_\mathrm{I}} \left(c_{\mathrm{CO_2\text{-}inj}} \cdot \overline{q}^n_{\mathrm{CO_2\text{-}inj},j} \right) \right\}, \tag{1}$$

where $\mathbf{u} = [u_1, u_2, \ldots, u_{N_\mathrm{u}}]^\mathrm{T} = [u^{1,1}, u^{1,2}, \ldots, u^{N_\mathrm{w}, N_\mathrm{c}}]^\mathrm{T}$ is the N_u-dimensional column vector that contains all the production and injection well controls, $u^{k,m}$ denotes the control of well k at the m^{th} control step, N_c is the number of control time steps, and N_w is the number of wells in total. In Eq. 1, Δt_n denotes the size of the n^{th} simulation time step, whereas t_n denotes the cumulative time at the end of the n^{th} time step; N_t, N_P, and N_I denote the number of time steps, number of producers, and number of injectors, respectively; $\overline{q}^n_{o,i}$, $\overline{q}^n_{w,i}$, and $\overline{q}^n_{\mathrm{CO_2\text{-}prd},i}$ denote the average oil production rate, average water production rate, and average CO_2 production rate of producer i over the n^{th} time step, respectively, whereas $\overline{q}^n_{\mathrm{CO_2\text{-}inj},j}$ denotes the average CO_2 injection rate of injector j over the n^{th} time step; c_o, c_w, $c_{\mathrm{CO_2\text{-}prd}}$, and $c_{\mathrm{CO_2\text{-}inj}}$ denote the oil price, produced water treatment cost, produced CO_2 treatment and capture cost, and CO_2 injection cost, respectively; b denotes the annual discount rate.

For a single-objective deterministic production optimization, the general nonlinearly constrained optimization problem for the NPV is defined as the nonlinear programming (NLP):

$$\underset{\mathbf{u}\in\mathbb{R}^{N_u}}{\text{minimize}} \quad J_{\mathrm{NPV}}(\mathbf{u}), \tag{2a}$$

$$\text{subject to:} \quad u_i^{\mathrm{low}} \le u_i \le u_i^{\mathrm{up}}, \qquad i = 1, 2, \ldots, N_\mathrm{u}, \tag{2b}$$

$$c_i(\mathbf{u}) \ge 0, \qquad i = 1, 2, \ldots, N_\mathrm{ic}. \tag{2c}$$

For the specific case study presented here in this paper, we consider the most common types of well controls, which are rate-controlled injectors and bottomhole-pressure-controlled producers. These well controls are subject to lower and upper bounds. The state constraints are imposed due to the limitation of the surface facilities, which are upper-bounded field liquid production rate (FLPR), and upper-bounded field water production rate (FWPR). In Eq. 2 and throughout this paper, u_i^{low} and u_i^{up} denote the lower and upper bounds of the i^{th} control variable, respectively, for the total of N_u variables; $c_i(\mathbf{u})$ denotes the general form of the i^{th} inequality constraint, with the total of N_ic inequality state constraints enforced in the reservoir model. It is important to note that $c_i(\mathbf{u})$ could be either linear or nonlinear, but without the loss of generality, we can assume them to be nonlinear. These nonlinear constraints are enforced at every control step, and their values are obtained from the simulation output.

In the context of carbon capture, utilization, and storage (CCUS), especially in the U.S., industrial companies who capture and store CO_2 will be provided carbon tax credits from the U.S. federal government to further incentivize investment in CCUS projects. These tax credits are also subject to monetary depreciation and inflation, therefore we should consider a separate objective function [40] of net present carbon tax credit (NPCTC), similar to the life-cycle NPV. To balance the two objectives at the same time, the maximization of both the life-cycle NPV and NPCTC are important. The negative NPCTC function is defined as

$$J_{\mathrm{NPCTC}}(\mathbf{u}) = -\sum_{n=1}^{N_t} \frac{\Delta t_n}{(1+b)^{\frac{t_n}{365}}} \left\{ \sum_{j=1}^{N_\mathrm{I}} \left(r_{\mathrm{CO_2}} \cdot \overline{q}^n_{\mathrm{CO_2\text{-}inj},j} \right) \right\}, \tag{3}$$

where $r_{\mathrm{CO_2}}$ denotes the carbon tax credit. The general bi-objective nonlinearly constrained production optimization problem is defined as

$$\underset{\mathbf{u}\in\mathbb{R}^{N_u}}{\text{minimize}} \quad \{J_{\mathrm{NPV}}(\mathbf{u}),\, J_{\mathrm{NPCTC}}(\mathbf{u})\}, \tag{4a}$$

$$\text{subject to:} \quad u_i^{\text{low}} \le u_i \le u_i^{\text{up}}, \qquad i = 1, 2, \ldots, N_{\text{u}}, \tag{4b}$$

$$c_i(\mathbf{u}) \ge 0, \qquad i = 1, 2, \ldots, N_{\text{ic}}. \tag{4c}$$

2.2 Normalization of the design variables and constraints

The magnitude of every design variable affects the performance of gradient-based optimization algorithms in general [4, 35]. Normalizing the design variables makes the step-size selection process stable, especially in a line-search method we used that will be discussed later in this paper. In our study, the design variables are min-max normalized using their original lower and upper bounds as

$$\bar{u}_i = \frac{u_i - u_i^{\text{low}}}{u_i^{\text{up}} - u_i^{\text{low}}}, \tag{5}$$

for all $i = 1, 2, \ldots, N_{\text{u}}$. After normalization, the normalized design variables $\bar{u}_i$ will have the lower and upper bound constraints to be 0 and 1, respectively. Likewise, to prevent numerical ill-conditioning caused by the difference in the magnitudes of the nonlinear constraint values, these constraints are normalized using the imposed lower or upper bound limits as the scaling factors. For example, the upper-bounded FLPR constraints are scaled by its upper limit value denoted by FLPR^{up}, so instead of directly enforcing the constraints given by

$$c_j(\bar{\mathbf{u}}) = -\text{FLPR}_j + \text{FLPR}^{\text{up}} \ge 0, \tag{6}$$

for each of the control time step j where $j = 1, 2, \ldots, N_{\text{c}}$, we enforce the following normalized constraints

$$\bar{c}_j(\bar{\mathbf{u}}) = -\frac{\text{FLPR}_j}{\text{FLPR}^{\text{up}}} + 1 \ge 0. \tag{7}$$

Therefore, the post-normalization single-objective optimization problem as shown in Eq. 2 becomes

$$\underset{\bar{\mathbf{u}} \in \mathbb{R}^{N_u}}{\text{minimize}} \quad J_{\text{NPV}}(\bar{\mathbf{u}}), \tag{8a}$$

$$\text{subject to:} \quad 0 \le \bar{u}_i \le 1, \qquad i = 1, 2, \ldots, N_{\text{u}}, \tag{8b}$$

$$\bar{c}_i(\bar{\mathbf{u}}) \ge 0, \qquad i = 1, 2, \ldots, N_{\text{ic}}. \tag{8c}$$

Likewise, the post-normalization bi-objective optimization problem given by Eq. 4 transforms to

$$\underset{\bar{\mathbf{u}} \in \mathbb{R}^{N_u}}{\text{minimize}} \quad \{J_{\text{NPV}}(\bar{\mathbf{u}}), J_{\text{NPCTC}}(\bar{\mathbf{u}})\}, \tag{9a}$$

$$\text{subject to:} \quad 0 \le \bar{u}_i \le 1, \qquad i = 1, 2, \ldots, N_{\text{u}}, \tag{9b}$$

$$\bar{c}_i(\bar{\mathbf{u}}) \ge 0, \qquad i = 1, 2, \ldots, N_{\text{ic}}. \tag{9c}$$

2.3 Lexicographic method

The lexicographic method is known as one of the most efficient ways to solve a multi-objective optimization problem [32]. Its basic idea is to solve multiple individual optimization problems whose number is equal to the number of objective functions. The order of which optimization problem to be solved first depends on the order of importance of the objective functions. Consider the following general multi-objective optimization problem consisting of n objective functions:

$$\underset{\bar{\mathbf{u}} \in \mathbb{R}^{N_u}}{\text{minimize}} \quad \{f_1(\bar{\mathbf{u}}), f_2(\bar{\mathbf{u}}), \ldots, f_n(\bar{\mathbf{u}})\}, \tag{10a}$$

$$\text{subject to:} \quad \bar{c}_i(\bar{\mathbf{u}}) \ge 0, \quad i = 1, 2, \ldots, N_{\text{cons}}, \tag{10b}$$

where N_{cons} represents the total number of inequality constraints in general, and in Eq. 10a, the objective functions are decreasingly ranked from the highest order of importance ($f_1(\bar{\mathbf{u}})$) to the lowest order of importance ($f_n(\bar{\mathbf{u}})$). The main idea of the lexicographic method is to sequentially solve n optimization problems in total. For every $k = 2, 3, \ldots, n$, the following k^{th} subproblem is solved:

$$\underset{\bar{\mathbf{u}} \in \mathbb{R}^{N_u}}{\text{minimize}} \quad f_k(\bar{\mathbf{u}}), \tag{11a}$$

$$\text{subject to:} \quad f_j(\bar{\mathbf{u}}) \le f_j(\bar{\mathbf{u}}_j^*), \qquad j = 1, 2, \ldots, (k-1), \tag{11b}$$

$$\bar{c}_i(\bar{\mathbf{u}}) \ge 0, \qquad i = 1, 2, \ldots, N_{\text{cons}}. \tag{11c}$$

Note that the constraint in Eq. 11b is not imposed for the first subproblem where $k = 1$, and in which $\bar{\mathbf{u}}_j^*$ denotes the optimal solution of every subproblem j prior to k for $j = 1, 2, \ldots, (k-1)$. Also, note that for $j \ge 2$, the functional value $f_j(\bar{\mathbf{u}}_j^*)$ is not necessarily the same as the independent single-objective optimal value of $f_j(\bar{\mathbf{u}})$ due to new additional constraints imposed on each j^{th} subproblem. In our case where we are focusing on a bi-objective problem as shown in Eq. 9 with the primary objective function being $J_{\text{NPV}}(\bar{\mathbf{u}})$, there are two optimization problems that need to be solved. The first step is to solve the single-objective NPV optimization problem as defined in Eq. 8 to determine the

optimal well controls $\bar{\mathbf{u}}^*$ and the corresponding optimal negative life-cycle NPV $J_{\mathrm{NPV}}(\bar{\mathbf{u}}^*)$. Then, we proceed to solve the second optimization problem to minimize the secondary objective function $J_{\mathrm{NPCTC}}(\bar{\mathbf{u}})$, subject to an additional constraint on the primary objective function $J_{\mathrm{NPV}}(\bar{\mathbf{u}})$, defined as follows:

$$\underset{\bar{\mathbf{u}}\in\mathbb{R}^{N_u}}{\text{minimize}} \quad J_{\mathrm{NPCTC}}(\bar{\mathbf{u}}), \tag{12a}$$

$$\text{subject to:} \quad J_{\mathrm{NPV}}(\bar{\mathbf{u}}) \leq \gamma J_{\mathrm{NPV}}(\bar{\mathbf{u}}^*), \tag{12b}$$

$$0 \leq \bar{u}_i \leq 1, \qquad i = 1, 2, \ldots, N_{\mathrm{u}}, \tag{12c}$$

$$\bar{c}_i(\bar{\mathbf{u}}) \geq 0, \qquad i = 1, 2, \ldots, N_{\mathrm{ic}}, \tag{12d}$$

where $\gamma \in (0, 1]$ is a preset value of relaxation or tolerance that indicates the fraction of decrease in life-cycle NPV (or increase in negative life-cycle NPV $J_{\mathrm{NPV}}(\bar{\mathbf{u}})$) that the operation is willing to sacrifice in order to exchange for an improvement (or decrease) in the secondary objective function. For example, if $\gamma = 0.95$ is selected, it means that the relaxation on the nonlinear state constraint given by Eq. 12b enforced on $J_{\mathrm{NPV}}(\bar{\mathbf{u}})$ would allow us to tolerate at most 5% increase in the negative life-cycle NPV, which is equivalent to 5% decrease in the life-cycle NPV, to further decrease the value of the negative NPCTC $J_{\mathrm{NPCTC}}(\bar{\mathbf{u}})$.

As stated previously, in [34], we showed that LS-SQP and TR-SQP optimization frameworks significantly outperform popular used ALM in nonlinearly constrained single-objective production optimization on a deterministic oil-water Brugge model [37]. This is the main motivation for us to utilize an SQP-based framework and extend it to multi-objective optimization. We also showed the similar convergence between our proposed LS-SQP and ∞-norm TR-SQP. Therefore, either one could be chosen as the main optimizer, and in this work, we choose LS-SQP. The details of the algorithm are described in a later section.

2.4 Stochastic Simplex Approximate Gradient (StoSAG)

The algorithm is introduced by [18] as a stochastic gradient approach based on N_{p} perturbations for robust optimization with geological uncertainty (N_{E} realizations). For our case, we only consider deterministic optimization with $N_{\mathrm{E}} = 1$, whose gradient is usually referred to as the "Simplex gradient" [17]. At each optimization iteration ν, we have the normalized design vector $\bar{\mathbf{u}}^\nu$ and the corresponding arbitrary objective function value $J(\bar{\mathbf{u}}^\nu)$. Note that in our specific case of bi-objective production optimization, the arbitrary objective function $J(\bar{\mathbf{u}})$ could be either $J_{\mathrm{NPV}}(\bar{\mathbf{u}})$ or $J_{\mathrm{NPCTC}}(\bar{\mathbf{u}})$. In the StoSAG procedures, each perturbation $\bar{\mathbf{u}}_{\mathrm{p}}$ is then assumed to be sampled from the normal distribution with mean $\bar{\mathbf{u}}^\nu$

$$\bar{\mathbf{u}}_{\mathrm{p}} \sim \mathcal{N}(\bar{\mathbf{u}}^\nu, \mathbf{C}_{\mathrm{U}}),$$

where $\mathbf{C}_{\mathrm{U}}$ is the block diagonal spherical covariance matrix with N_{w} blocks and each block sub-matrix, $\mathbf{C}_{\mathrm{U}}^{\mathrm{w}}$, corresponds to the correlation matrix over N_{c} control steps of well w whose elements are normally computed from a spherical covariance function given by

$$\mathbf{C}_{\mathrm{U},i,j}^{\mathrm{w}} = \begin{cases} \sigma^2 \left[1 - \frac{3}{2}\frac{h}{L} + \frac{1}{2}\left(\frac{h}{L}\right)^3\right], & h \leq L, \\ 0, & h > L, \end{cases} \tag{13}$$

where σ is the standard deviation of the perturbations (or referred to as the perturbation size) for the normalized design variables within the interval of $[0, 1]$, $h = |t_i - t_j|$, where t_i and t_j represent the times corresponding to the middle of the i^{th} and j^{th} control step intervals, respectively, and L is the temporal correlation length which we wish the control variables of well w to be correlated.

For each perturbation vector $\bar{\mathbf{u}}_{\mathrm{p}}$, we can evaluate the corresponding objective function $J(\bar{\mathbf{u}}_{\mathrm{p}})$. We can then form the corresponding $N_{\mathrm{u}} \times N_{\mathrm{p}}$ perturbation matrix

$$\Delta\mathbf{U}_{\mathrm{p}}^\nu = \left[(\bar{\mathbf{u}}_1^\nu - \bar{\mathbf{u}}^\nu), (\bar{\mathbf{u}}_2^\nu - \bar{\mathbf{u}}^\nu), \ldots, (\bar{\mathbf{u}}_{N_{\mathrm{p}}}^\nu - \bar{\mathbf{u}}^\nu)\right], \tag{14}$$

and the $N_{\mathrm{p}} \times 1$ perturbed objective function vector

$$\Delta\mathbf{j}_{\mathrm{p}}^\nu = \left[(J(\bar{\mathbf{u}}_1^\nu) - J(\bar{\mathbf{u}}^\nu)), (J(\bar{\mathbf{u}}_2^\nu) - J(\bar{\mathbf{u}}^\nu)), \ldots, (J(\bar{\mathbf{u}}_{N_{\mathrm{p}}}^\nu) - J(\bar{\mathbf{u}}^\nu))\right]^{\mathrm{T}}. \tag{15}$$

The stochastic gradient of the objective function could be then computed as

$$\nabla J(\bar{\mathbf{u}}^\nu) = \left[\left(\Delta\mathbf{U}_{\mathrm{p}}^\nu\right)^{\mathrm{T}}\right]^\dagger \Delta\mathbf{j}_{\mathrm{p}}^\nu, \tag{16}$$

where the superscript † denotes the Moore-Penrose pseudo-inverse [33, 36]. Note that we can use Eq. 15 to form the $N_{\mathrm{p}} \times 1$ perturbation vectors $\Delta\mathbf{j}_{\mathrm{NPV,p}}^\nu$ and $\Delta\mathbf{j}_{\mathrm{NPCTC,p}}^\nu$ for the two corresponding objective functions $J_{\mathrm{NPV}}(\bar{\mathbf{u}}^\nu)$ or $J_{\mathrm{NPCTC}}(\bar{\mathbf{u}}^\nu)$, respectively. The same approach could be used to compute each of the nonlinear constraint gradients $\nabla\bar{c}_i(\bar{\mathbf{u}}^\nu)$. For each of the nonlinear constraint $\bar{c}_i(\bar{\mathbf{u}}^\nu)$, where $i = 1, 2, \ldots, N_{\mathrm{ic}}$, we can compute the following $N_{\mathrm{p}} \times 1$ perturbation vector:

$$\Delta\bar{\mathbf{c}}_{i,\mathrm{p}}^\nu = \left[\left(\bar{c}_i(\bar{\mathbf{u}}_1^\nu) - \bar{c}_i(\bar{\mathbf{u}}^\nu)\right), \left(\bar{c}_i(\bar{\mathbf{u}}_2^\nu) - \bar{c}_i(\bar{\mathbf{u}}^\nu)\right), \ldots, \left(\bar{c}_i(\bar{\mathbf{u}}_{N_{\mathrm{p}}}^\nu) - \bar{c}_i(\bar{\mathbf{u}}^\nu)\right)\right]^{\mathrm{T}}, \tag{17}$$

which could be used directly in Eq. 16 instead of $\Delta\mathbf{j}_{\mathrm{p}}^{\nu}$ to compute the stochastic gradient $\nabla\bar{c}_i(\bar{\mathbf{u}}^{\nu})$. Algorithm 1 summarizes the overall StoSAG procedures.

Algorithm 1 StoSAG for nonlinearly constrained bi-objective optimization problem

1. Preset the number of perturbations N_{p}, the perturbation size σ, and the temporal correlation length L. Generate the block-diagonal covariance matrix $\mathbf{C}_{\mathrm{U}}$ from spherical variogram given by Eq. 13.
2. Sample the perturbations $\bar{\mathbf{u}}_{\mathrm{p}} \sim \mathcal{N}(\bar{\mathbf{u}}^{\nu}, \mathbf{C}_{\mathrm{U}})$. Construct the $N_{\mathrm{u}} \times N_{\mathrm{p}}$ perturbation matrix $\Delta\mathbf{U}_p^{\nu}$ as described in Eq. 14.
3. Construct the $N_{\mathrm{p}} \times 1$ perturbation vectors $\Delta\mathbf{j}_{\mathrm{NPV,p}}^{\nu}$ and $\Delta\mathbf{j}_{\mathrm{NPCTC,p}}^{\nu}$ using Eq. 15. Compute the objective function gradients $\nabla J_{\mathrm{NPV}}(\bar{\mathbf{u}}^{\nu})$ and $\nabla J_{\mathrm{NPCTC}}(\bar{\mathbf{u}}^{\nu})$ using Eq. 16.
4. For each nonlinear constraint $\bar{c}_i(\bar{\mathbf{u}}^{\nu})$, where $i = 1, 2, \ldots, N_{\mathrm{ic}}$, construct the $N_{\mathrm{p}} \times 1$ perturbation vector $\Delta\bar{\mathbf{c}}_{i,\mathrm{p}}^{\nu}$ using Eq. 17, and compute the nonlinear constraint gradient $\nabla\bar{c}_i(\bar{\mathbf{u}}^{\nu})$ using Eq. 16 with $\Delta\bar{\mathbf{c}}_{i,\mathrm{p}}^{\nu}$ instead of $\Delta\mathbf{j}_{\mathrm{p}}^{\nu}$.

2.5 Line-search Sequential Quadratic Programming (LS-SQP)

As introduced in [34], the Line-search Sequential Quadratic Programming (LS-SQP) coupled with StoSAG gradients is a powerful and efficient method to solve the nonlinearly constrained deterministic optimization problems. Consider the following post-normalization optimization problem:

$$\underset{\bar{\mathbf{u}}\in\mathbb{R}^{N_u}}{\text{minimize}} \quad J(\bar{\mathbf{u}}), \tag{18a}$$

$$\text{subject to:} \quad \bar{c}_i(\bar{\mathbf{u}}) \geq 0, \qquad i = 1, 2, \ldots, N_{\mathrm{cons}}, \tag{18b}$$

where the arbitrary objective function $J(\bar{\mathbf{u}})$ could be either $J_{\mathrm{NPV}}(\bar{\mathbf{u}})$ or $J_{\mathrm{NPCTC}}(\bar{\mathbf{u}})$. Similar to what has been defined in Eq. 11, N_{cons} is the total number of inequality constraints, which accounts for the fact that each individual bound constraint from the general optimization problem defined in Eqs. 8, 9, and 12 has been decomposed into two corresponding general linear inequality constraints. Note that in the lexicographic method, we have $N_{\mathrm{cons}} = (N_{\mathrm{ic}} + 2N_{\mathrm{u}})$ for the first-step single-objective optimization problem defined by Eq. 8, whereas $N_{\mathrm{cons}} = (N_{\mathrm{ic}} + 2N_{\mathrm{u}} + 1)$ for the second-step optimization problem given by Eq. 12 as there is an additional state constraint imposed on $J_{\mathrm{NPV}}(\bar{\mathbf{u}})$. To solve the general NLP as given by Eq. 18, the Lagrangian is firstly defined as

$$L(\bar{\mathbf{u}}, \boldsymbol{\lambda}) = J(\bar{\mathbf{u}}) - \sum_{i=1}^{N_{\mathrm{cons}}} \lambda_i \bar{c}_i(\bar{\mathbf{u}}), \tag{19}$$

where $\boldsymbol{\lambda} = \left[\lambda_1, \lambda_2, ..., \lambda_{N_{\mathrm{cons}}}\right]^{\mathrm{T}}$ is a N_{cons}-dimensional column vector consisting of the Lagrange multipliers for each of the corresponding inequality constraints. The Lagrange dual problem of the NLP given by Eq. 18 is as follows:

$$\underset{\boldsymbol{\lambda}\in\mathbb{R}^{N_{\mathrm{cons}}}}{\text{maximize}} \quad \left(\underset{\bar{\mathbf{u}}\in\mathbb{R}^{N_u}}{\text{minimize}} \quad L(\bar{\mathbf{u}}, \boldsymbol{\lambda})\right), \tag{20a}$$

$$\text{subject to:} \quad \bar{c}_i(\bar{\mathbf{u}}) \geq 0, \qquad i = 1, 2, \ldots, N_{\mathrm{cons}}. \tag{20b}$$

Successfully solving the dual problem defined by Eq. 20 provides the lower bound of the optimal solution of the original primal problem given by Eq. 18. When strong duality holds, both the primal optimality and dual optimality are equal to each other [35]. The first order optimality conditions, or Karush-Kuhn-Tucker (KKT) conditions, associated with the dual problem Eq. 20, are given by

$$\nabla_{\bar{\mathbf{u}}} L(\bar{\mathbf{u}}, \boldsymbol{\lambda}) = 0, \tag{21a}$$

$$\bar{c}_i(\bar{\mathbf{u}}) \geq 0, \qquad i = 1, 2, ..., N_{\mathrm{cons}}, \tag{21b}$$

$$\lambda_i \geq 0, \qquad i = 1, 2, ..., N_{\mathrm{cons}}, \tag{21c}$$

$$\lambda_i \bar{c}_i(\bar{\mathbf{u}}) = 0, \qquad i = 1, 2, ..., N_{\mathrm{cons}}. \tag{21d}$$

Sequential Quadratic Programming (SQP) is known as a powerful family of methods to handle the nonlinear minimization problem as described by Eq. 20 by sequentially satisfying the KKT conditions at each iteration. The basic idea of SQP methods is to linearize the KKT conditions at the current iteration $(\nu + 1)$ using the information from the previous iteration ν. The linearized KKT conditions [4, 35] for the original KKT equations defined by Eq. 21 are given by

$$\mathbf{H}^{\nu}\mathbf{d}^{\nu} + \nabla J(\bar{\mathbf{u}}^{\nu}) - \left(\mathbf{A}_c^{\nu}\right)^{\mathrm{T}} \boldsymbol{\lambda}^{\nu+1} = 0, \tag{22a}$$

$$\left(\nabla\bar{c}_i(\bar{\mathbf{u}}^{\nu})\right)^{\mathrm{T}} \mathbf{d}^{\nu} + \bar{c}_i(\bar{\mathbf{u}}^{\nu}) \geq 0, \qquad i = 1, 2, \ldots, N_{\mathrm{cons}}, \tag{22b}$$

$$\lambda_i^{\nu+1} \geq 0, \qquad i = 1, 2, \ldots, N_{\mathrm{cons}}, \tag{22c}$$

$$\lambda_i^{\nu+1}\left[\bar{c}_i(\bar{\mathbf{u}}^{\nu}) + \left(\nabla\bar{c}_i(\bar{\mathbf{u}}^{\nu})\right)^{\mathrm{T}} \mathbf{d}^{\nu}\right] = 0, \qquad i = 1, 2, \ldots, N_{\mathrm{cons}}, \tag{22d}$$

where $\mathbf{H}^{\nu}$ is the Hessian matrix of the Lagrangian function defined by Eq. 19 at the previous iteration ν, $\mathbf{A}_c^{\nu} = \left[\nabla\bar{c}_1(\bar{\mathbf{u}}^{\nu}), \nabla\bar{c}_2(\bar{\mathbf{u}}^{\nu}), ..., \nabla\bar{c}_{N_{\mathrm{cons}}}(\bar{\mathbf{u}}^{\nu})\right]^{\mathrm{T}}$ is the $N_{\mathrm{cons}} \times N_{\mathrm{u}}$ Jacobian matrix of the inequality constraints, and $\mathbf{d}^{\nu} = \bar{\mathbf{u}}^{\nu+1} - \bar{\mathbf{u}}^{\nu}$ is the update vector of the design variables. At each optimization itereation, the following quadratic programming (QP) subproblem [35] is solved:

$$\underset{\mathbf{d}^{\nu}\in\mathbb{R}^{N_u}}{\text{minimize}} \quad \frac{1}{2}\left(\mathbf{d}^{\nu}\right)^{\mathrm{T}} \mathbf{H}^{\nu}\mathbf{d}^{\nu} + \left[\nabla J(\bar{\mathbf{u}}^{\nu})\right]^{\mathrm{T}} \mathbf{d}^{\nu}, \tag{23a}$$

$$\text{subject to:} \quad \mathbf{A}_c^{\nu}\mathbf{d}^{\nu} + \bar{\mathbf{c}}(\bar{\mathbf{u}}^{\nu}) \geq 0, \tag{23b}$$

where $\bar{\mathbf{c}}(\bar{\mathbf{u}}^\nu) = \left[\bar{c}_1(\bar{\mathbf{u}}^\nu), \bar{c}_2(\bar{\mathbf{u}}^\nu), \ldots, \bar{c}_{N_{\text{cons}}}(\bar{\mathbf{u}}^\nu)\right]^{\mathrm{T}}$ is the vector consisting of all inequality constraints. Once the QP search direction $\mathbf{d}^\nu$ has been successfully solved, the corresponding Lagrange multipliers [4] can be computed from Eq. 22a as

$$\hat{\boldsymbol{\lambda}}^{\nu+1} = [\mathbf{A}_{ac}\,(\mathbf{A}_{ac})^{\mathrm{T}}]^{-1}\mathbf{A}_{ac}\left[\mathbf{H}^\nu\mathbf{d}^\nu + \nabla J(\bar{\mathbf{u}}^\nu)\right], \tag{24}$$

where $\hat{\boldsymbol{\lambda}}^{\nu+1}$ and $\mathbf{A}_{ac}$ denote the vector of Lagrange multipliers and the Jacobian of the active linearized inequality constraints given in Eq. 22b, respectively. Note that $\mathbf{A}_{ac}$ is a sub-matrix of the full Jacobian matrix $\mathbf{A}_c^\nu$. Moreover, we can reconstruct the the full Lagrange multiplier vector $\boldsymbol{\lambda}^{\nu+1}$ by reinserting zeroes into $\hat{\boldsymbol{\lambda}}^{\nu+1}$ wherever appropriate.

A general NLP can be viewed as a bi-objective numerical optimization problem, in which we opt to minimize both the original objective function and the constraint violation. The LS-SQP approach introduced by [34] combines both said objectives into a single merit function, formulated as follows:

$$\begin{aligned}\Phi(\bar{\mathbf{u}}^\nu + \alpha\mathbf{d}^\nu) = {} & J(\bar{\mathbf{u}}^\nu + \alpha\mathbf{d}^\nu) \\ & - \sum_{i=1}^{N_{\text{cons}}} \lambda_i^{\nu+1} \min\left\{\bar{c}_i(\bar{\mathbf{u}}^\nu + \alpha\mathbf{d}^\nu), 0\right\},\end{aligned} \tag{25}$$

where α denotes the backtracking step size for the line-search procedure. The minimum operator on the right-hand side of Eq. 25 is to prevent from over-penalizing inviolate (or satisfied) constraints. During backtracking, the step size is inexactly solved by reducing by a predefined factor ρ (detailed in Algorithm 2) if the following Armijo-Goldstein condition [4, 35] is not satisfied:

$$\Phi(\bar{\mathbf{u}}^\nu + \alpha\mathbf{d}^\nu) \leq \Phi(\bar{\mathbf{u}}^\nu) + \eta\alpha D(\Phi(\bar{\mathbf{u}}^\nu), \mathbf{d}^\nu), \tag{26}$$

where $\eta \in (0, 1)$ is a small positive constant. The operator $D(\Phi(\bar{\mathbf{u}}^\nu), \mathbf{d}^\nu)$ is the directional derivative of the merit function $\Phi(\bar{\mathbf{u}}^\nu)$ along the search direction $\mathbf{d}^\nu$, which is defined in [34] as

$$\begin{aligned}D(\Phi(\bar{\mathbf{u}}^\nu), \mathbf{d}^\nu) &= \left(\nabla\Phi(\bar{\mathbf{u}}^\nu)\right)^{\mathrm{T}}\mathbf{d}^\nu \\ &= \left[\left(\nabla J(\bar{\mathbf{u}}^\nu)\right)^{\mathrm{T}} - \left(\boldsymbol{\lambda}^{\nu+1}\right)^{\mathrm{T}}\mathbf{A}_c^\nu\right]\mathbf{d}^\nu.\end{aligned} \tag{27}$$

It is crucial to note that the Lagrange multiplier vector $\boldsymbol{\lambda}^{\nu+1}$ has been computed as if the operation takes the full QP search direction $\mathbf{d}^\nu$ from Eq. 22a. In such case, some of the linearized inequality constraints could be set active [34]. Due to this fact, the vector $\boldsymbol{\lambda}^{\nu+1}$ might contain zero values, which do not contribute to the penalty term indicated by the summation in the merit function defined by Eq. 25. Therefore, it is necessary to perform the following secondary violation check:

$$\bar{c}_j(\bar{\mathbf{u}}^\nu + \alpha\mathbf{d}^\nu) \geq 0, \qquad \forall j \in J : \lambda_j^{\nu+1} = 0. \tag{28}$$

This step is to ensure that the inequality constraints associated with the zero-valued Lagrange multipliers are not violated [34]. Algorithm 2 summarizes the LS-SQP backtracking procedure by [34]. At every LS-SQP optimization iteration ν, the Hessian matrix of the Lagrangian $\mathbf{H}^\nu$ is updated using the Damped Broyden-Fletcher-Goldfarb-Shanno (Damped BFGS) algorithm [4, 35]. The complete workflow of the LS-SQP algorithm coupled with StoSAG gradients for general nonlinearly constrained production optimization problem is summarized in Algorithm 3 and Fig. 1.

Algorithm 2 Backtracking

1. Initialize initial step size $\alpha = \alpha_{\max}$, step size reduction factor ρ, and maximum number of step size cut $n_{\text{cuts, max}}$. Choose the small constant parameter $\eta \in (0, 1)$. Set the step size cut counter $n_{\text{cuts}} = 0$.
2. Extract the subset $J = \left\{j \in J : \lambda_j^{\nu+1} = 0\right\}$ from the Lagrange multiplier vector $\boldsymbol{\lambda}^{\nu+1}$ computed from Eq. 24.
3. WHILE $\left\{\Phi(\bar{\mathbf{u}}^\nu + \alpha\mathbf{d}^\nu) > \Phi(\bar{\mathbf{u}}^\nu) + \eta\alpha D(\Phi(\bar{\mathbf{u}}^\nu), \mathbf{d}^\nu)\right.$ **OR** $\left.\exists j \in J : \bar{c}_j(\bar{\mathbf{u}}^\nu + \alpha\mathbf{d}^\nu) < 0\right\}$ **AND** $n_{\text{cuts}} \leq n_{\text{cuts, max}}$:
   - Step size reduction: $\alpha \leftarrow \rho\alpha$.
   - Set backtracking cut counter: $n_{\text{cuts}} \leftarrow n_{\text{cuts}} + 1$.
   - Loop.
4. If backtracking succeeds, return the step size α and the actual search direction $\mathbf{d}^\nu \leftarrow \alpha\mathbf{d}^\nu$.

3 Reservoir model description

In this section, we describe the reservoir model and optimization settings used to apply the proposed methodology to perform bi-objective optimization of CO_2 storage into an oil reservoir.

3.1 Physical model

In this study, we perform bi-objective optimization on the Brugge model. The Brugge model is originally an oil-water synthetic reservoir model created by TNO as a comparative study for closed-loop reservoir management [37], which consists of 104 different realizations due to geological uncertainty. The reservoir model has 60,048 gridblocks with a total of 30 wells - 10 injectors and 20 producers ($N_{\text{I}} = 10$, $N_{\text{P}} =$

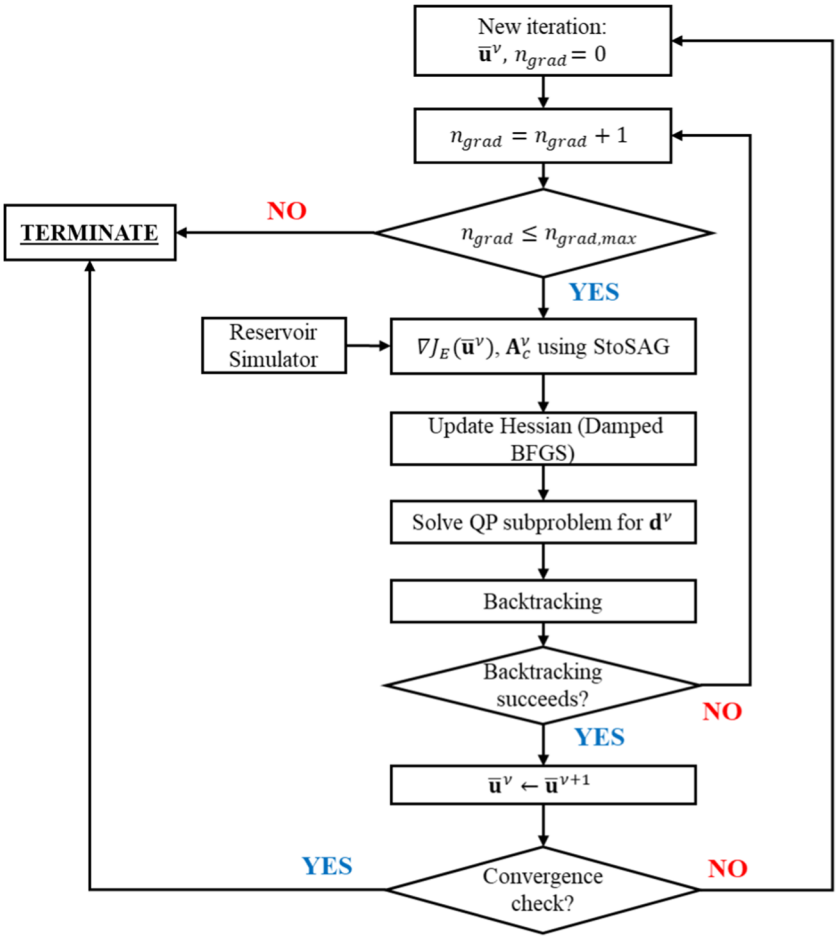

Fig. 1 Simplified flowchart of the LS-SQP algorithmic framework

20), as shown in Fig. 2. In this study, we only consider the base case (58th realization) for deterministic production optimization. Additionally, for the purpose of simulating the CO_2 utilization and storage processes, the Brugge model has been modified from the original oil-water model to a compositional model, simulated using CMG-GEM commercial compositional reservoir simulator. During the simulation process, as the producers are located at the center of the reservoir model and are surrounded by the injectors, the CO_2 injection displaces the in-situ fluids towards the central area for production and stays trapped, both in the pore spaces and via dissolution.

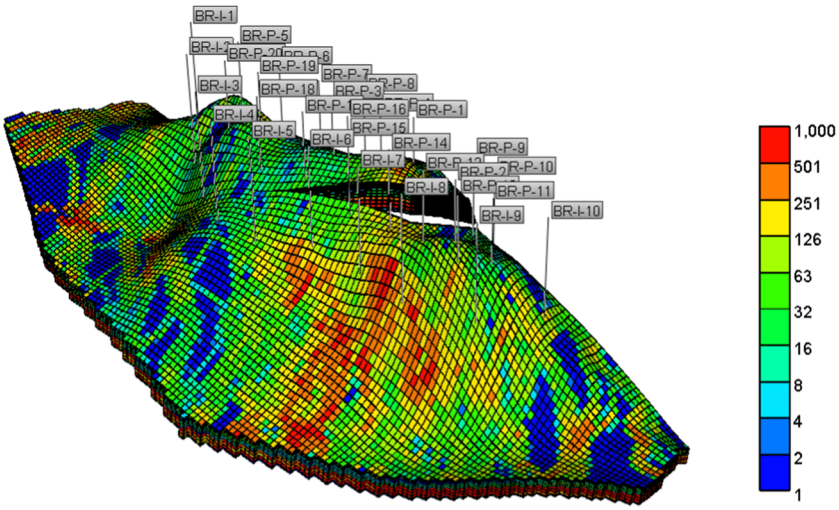

Fig. 2 Three-dimensional log-permeability visualization (units: mD) of the Brugge reservoir model with 30 wells

The initial reservoir pressure is 3, 500 psi, and the compositional fluid model is similar to the one used in [42]. For more details regarding the compositional data, please refer to Table 4 and Table 5 in the **Appendix A**.Note that there is still some oil production in the system, which is a major reason for considering a multi-objective optimization solution in this work.

Algorithm 3 LS-SQP algorithm coupled with StoSAG gradients for production optimization

1. Preset maximum number of gradient recomputations $n_{\text{grad,max}}$, maximum number of backtracking cuts $n_{\text{cuts,max}}$, maximum backtracking step size $\alpha_{\max}$, step size reduction factor ρ, objective function change tolerance ϵ_{J}, design vector change tolerance ϵ_{u}, and the maximum number of optimization iterations N_{iter}. Specify the number of perturbations N_{p}, the perturbation size σ, and the temporal correlation length L for StoSAG.
2. Initialize the following: optimization iteration index $\nu = 0$, the normalized well control vector $\bar{\mathbf{u}}^0$, and the Hessian matrix $\mathbf{H}^0 = \mathbf{I}_{N_{\text{u}}}$ where $\mathbf{I}_{N_{\text{u}}}$ is the $N_{\text{u}} \times N_{\text{u}}$ identity matrix.
3. Set the gradient counter $n_{\text{grad}} = 1$, backtracking cut counter $n_{\text{cuts}} = 0$, and a boolean variable ResetH = **FALSE**.
4. Compute the objective function gradient $\nabla J(\bar{\mathbf{u}}^\nu)$, and the constraint Jacobian matrix $\mathbf{A}_c^\nu$ using the StoSAG procedures in Algorithm 1.
5. QP solver for the search direction $\mathbf{d}^\nu$:
   (a) Hessian matrix update:
   - If ResetH = **FALSE**, update the Hessian matrix $\mathbf{H}^\nu$ using Damped BFGS procedure [4, 35].
   - Else, skip this step and proceed to Step 5b.

   (b) Solve the QP subproblem given by Eq. 23 for the search direction $\mathbf{d}^\nu$. If the QP subproblem is infeasible, set $n_{\text{grad}} \leftarrow n_{\text{grad}} + 1$ and go back to Step 4 to recompute the stochastic gradients. If $n_{\text{grad}} = n_{\text{grad,max}}$ then:
   - If ResetH = **FALSE**, go to Step 8.
   - Else, terminate the algorithm.

   (c) Go to Step 6 if the QP search direction $\mathbf{d}^\nu$ from Step 5b has been computed successfully.
6. Compute the associated Lagrange multiplier vector $\boldsymbol{\lambda}^{\nu+1}$ from Eq. 24, then go to Step 7.
7. Perform backtracking as described in Algorithm 2 to find the step size α and the actual search direction. If backtracking succeeds, go to Step 9, else set $n_{\text{grad}} \leftarrow n_{\text{grad}} + 1$ and go back to Step 4. If $n_{\text{grad}} = n_{\text{grad,max}}$ then:
   - If ResetH = **FALSE**, go to Step 8.
   - Else, terminate the algorithm.
8. Set ResetH = **TRUE**, reset the Hessian matrix to the identity matrix $\mathbf{I}_{N_{\text{u}}}$, reset $n_{\text{grad}} = 1$ and go back to Step 4.
9. Return the line-search step size α and the corresponding actual search direction $\mathbf{d}^\nu \leftarrow \alpha \mathbf{d}^\nu$ from backtracking procedure in Algorithm 2. Recompute the actual Lagrange multiplier vector $\boldsymbol{\lambda}^{\nu+1}$ using this actual search direction in Eq. 24. Set $\bar{\mathbf{u}}^{\nu+1} = \bar{\mathbf{u}}^\nu + \mathbf{d}^\nu$ and return the objective function value $J(\bar{\mathbf{u}}^{\nu+1})$. Go to Step 10.
10. Check for convergence criteria:

$$\frac{\left|J(\bar{\mathbf{u}}^{\nu+1}) - J(\bar{\mathbf{u}}^\nu)\right|}{|J(\bar{\mathbf{u}}^\nu)|} \leq \epsilon_{\text{J}} \quad \textbf{AND} \quad \|\bar{\mathbf{u}}^{\nu+1} - \bar{\mathbf{u}}^\nu\|_2 \leq \epsilon_{\text{u}}$$

- If not converged, save the following parameters as prior information: $\nabla J(\bar{\mathbf{u}}^\nu)$, $\mathbf{A}_c^\nu$, $\mathbf{H}^\nu$, and $\boldsymbol{\lambda}^{\nu+1}$ as these variables are needed for Damped BFGS update in Step 5a. Increment $\nu \leftarrow \nu + 1$ and go back to Step 3.
- Else, terminate the algorithm.

Table 1 Lower and upper limits of the well controls

Variable	Units	Lower limit	Upper limit
Production BHP	psi	1,000	3,000
CO_2 injection rate	MMscf/d	10	15

3.2 Optimization settings

In our study, we consider a 3600-day life-cycle production optimization, with 20 uniform control steps of 180 days each. Hence, the number of control variables in this bi-objective optimization problem is 600, and their lower and upper bounds are given in Table 1. The enforced nonlinear state constraints are shown in Table 2.

Table 3 summarizes the economical values that are used in the objective functions defined by Eqs. 1 and 3. For the carbon-related parameters specifically, please refer to [38], [23], and [39]. The parameter settings for the LS-SQP framework by [34], as shown in Algorithm 3, are summarized in Table 6 in the **Appendix A**.

4 Computational results

In this section, we present our computation results obtained by applying the methodology introduced in this work on the compositional Brugge model.

4.1 Single-objective production optimization

As explained earlier previously, performing bi-objective production optimization with the lexicographic method requires the solution of the single-objective NPV optimization problem as defined by Eq. 8. The well controls are uniformly initialized as $\bar{u}_i^0 = 0.5$ for all $i = 1, 2, \ldots, N_{\text{u}}$ (midpoint initialization). The NPV optimization results are shown in Fig. 3, while the optimal well controls ($\bar{\mathbf{u}}^*$ in Eq. 12) are shown as heatmap schedules in Fig. 4. It can be seen that the LS-SQP framework solves the NPV optimization problem after 57 optimization iterations, which corresponds to 1, 248 objective function evaluation (reservoir simulation)

Table 2 Summary of the imposed nonlinear state constraints

Constraint Type	Units	Type of inequality	Value
FLPR	stb/d	$\leq$ (upper-bounded)	50,000
FWPR	stb/d	$\leq$ (upper-bounded)	7,000

Table 3 Summary of the economical parameters used in the objective functions

Economic Parameter	Notation	Units	Value
Oil price	c_o	\$/stb	82
Water treatment cost	c_w	\$/stb	5
CO_2 injection cost	$c_{CO_2\text{-inj}}$	$/tCO$_2^{(*)}$	10
CO_2 capture cost	$c_{CO_2\text{-prd}}$	$/tCO$_2^{(*)}$	47
Carbon tax credit	r_{CO_2}	$/tCO$_2^{(*)}$	35
Annual discount rate	b	fraction	0.1

(∗): tCO_2 = metric ton of CO_2

calls. The optimal NPV found by LS-SQP is $NPV_{max} = -J_{NPV}(\bar{\mathbf{u}}^*) = 10.04 \times 10^9$ USD.

Figure 5 shows the values of the nonlinear state constraints (FLPR and FWPR) imposed on the optimization problem. We can see that the LS-SQP algorithm honors these constraints very well with no violation at the optimum $\bar{\mathbf{u}}^*$. It can be observed that the maximum value of FLPR is obtained at the first control step, while the maximum FWPR is observed at the second control step.

4.2 Bi-objective production optimization

Here, we demonstrate the performance of the LS-SQP framework in solving the NPCTC optimization problem, or the second-step lexicographic optimization problem as given by Eq. 12. Note that for this optimization problem, the design vector is initialized at the solution of the single-objective optimum $\bar{\mathbf{u}}^*$ found previously, since it is the most feasible solution that satisfy all the imposed constraints. The negative-NPV state constraint given by Eq. 12b is upper-bounded using the value of $J_{NPV}(\bar{\mathbf{u}}^*) = -10.04 \times 10^9$ USD, while the initial negative NPCTC objective function value is $J_{NPCTC}(\bar{\mathbf{u}}^*) = -5.12 \times 10^8$ USD.

The optimization results are shown for $\gamma = 0.99$, which corresponds to the maximum allowance of 1% increase in the negative life-cycle NPV function $J_{NPV}(\bar{\mathbf{u}})$. The motivation for this choice of γ value, rather than exactly equal to 1 in the formal formulation of the lexicographic method defined by Eq. 11, is for the purposes of allowing a small tolerance window in the NPV state constraint that still ensures the numerical stability due to the errors in stochastic gradient estimations. Also, as $\gamma = 0.99$ is very close to 1, it is a good representative value to benchmark the performance of our proposed methodology to confirm we achieve solution feasibility at the end of optimization.

Figure 6 shows the bi-objective optimization results for the NPCTC and NPV, in which the green dashed lines represent the upper bound $\gamma J_{NPV}(\bar{\mathbf{u}}^*)$ of the negative NPV constraint (or lower bound of the NPV). The LS-SQP framework successfully optimizes the two objective functions after 71 optimization iterations, corresponding to 1,064 reservoir simulation calls, which results in the optimal NPCTC of $J_{NPCTC}(\bar{\mathbf{u}}_{opt}) = -5.826 \times 10^8$ USD. It can be observed from Figure 6 that for most iterations, the NPV state constraint Eq. 12b is violated as the NPV is lower than the NPV bound. It is worth noting that during intermediate optimization iterations, the solver does not have to always guarantee constraint feasibility. Although not shown here, our numerical experiments confirm that rigorously enforcing the solution to always be feasible at every optimization iteration would yield a suboptimal result, as good directions that make good progress are repeatedly rejected, eventually forcing the optimizer to stop. Thus, by allowing some small violations during intermediate iterations, we can achieve much better convergence. The solver will always try to gradually restore feasibility at later iterations, whose speed depends on the quality of the stochastic gradient estimation. Despite such said inaccuracy, at the optimum, the LS-SQP algorithm is still able to restore the NPV constraint feasibility.

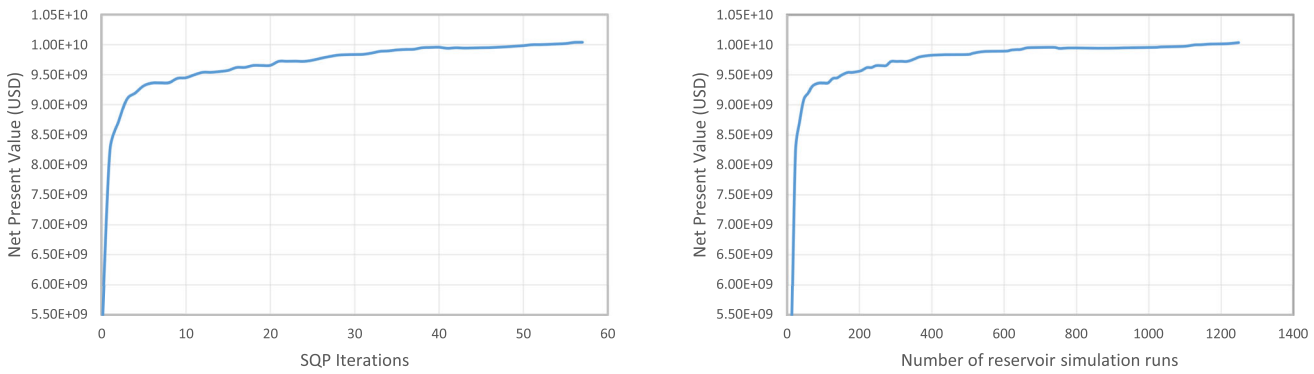

(a) NPV vs number of iterations

(b) NPV vs. number of reservoir simulations

Fig. 3 Single-objective NPV optimization results using the LS-SQP workflow: (a) NPV vs. number of iterations and (b) NPV vs. number of reservoir simulation runs

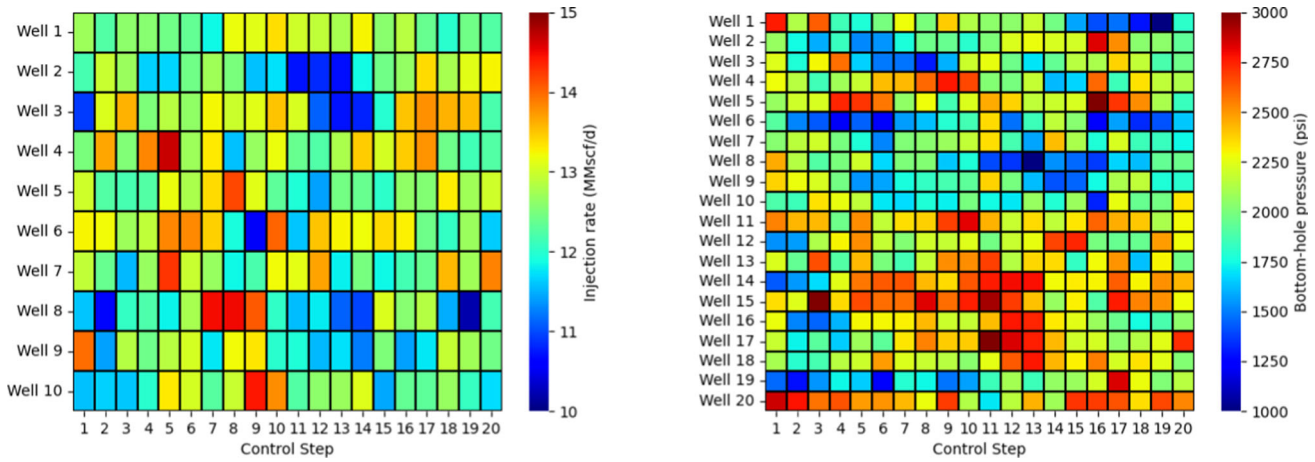

(a) Injection **(b)** Production

Fig. 4 Optimal well control schedules for the single-objective NPV optimization problem: (a) Injection rates for 10 wells and (b) Bottom-hole pressures for 20 producers

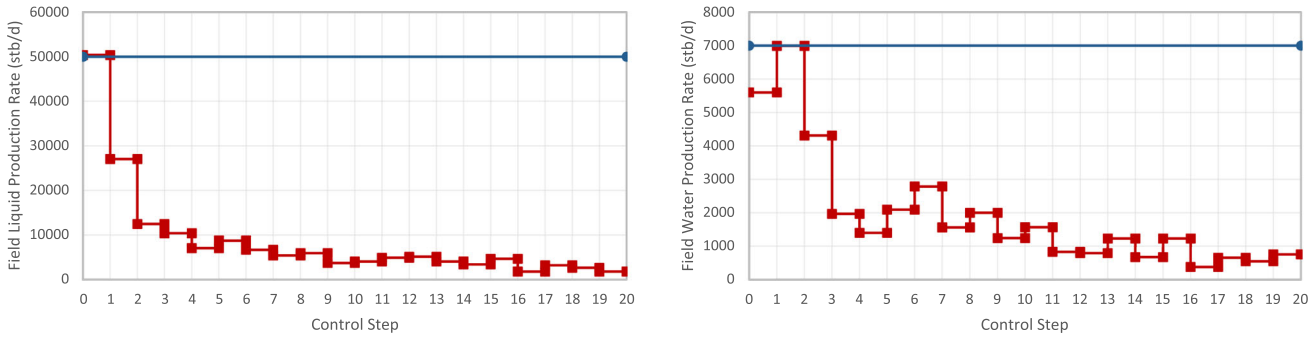

(a) Field liquid production rate (FLPR) **(b)** Field water production rate (FWPR)

Fig. 5 Enforced nonlinear constraint values at the optimum of the single-objective problem: (a) Field liquid production rate vs. control steps and (b) Field water production rate vs. control steps

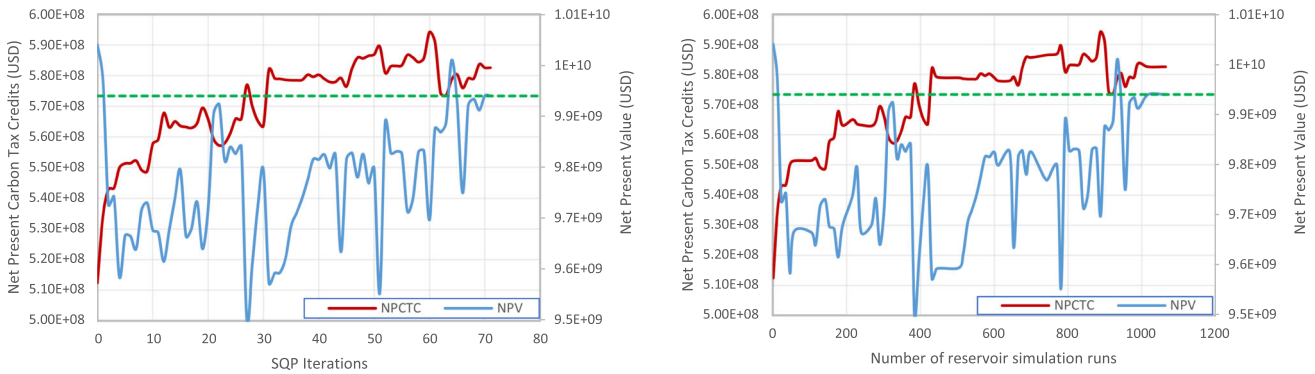

(a) NPCTC and NPV vs. number of iterations **(b)** NPCTC and NPV vs. number of reservoir simulations

Fig. 6 Bi-objective NPCTC and NPV optimization results for $\gamma = 0.99$: (a) NPCTC and NPV vs. number of iterations and (b) NPCTC and NPV vs. number of reservoir simulation runs. The green dashed lines in both figures indicate the lower bound of NPV state constraint

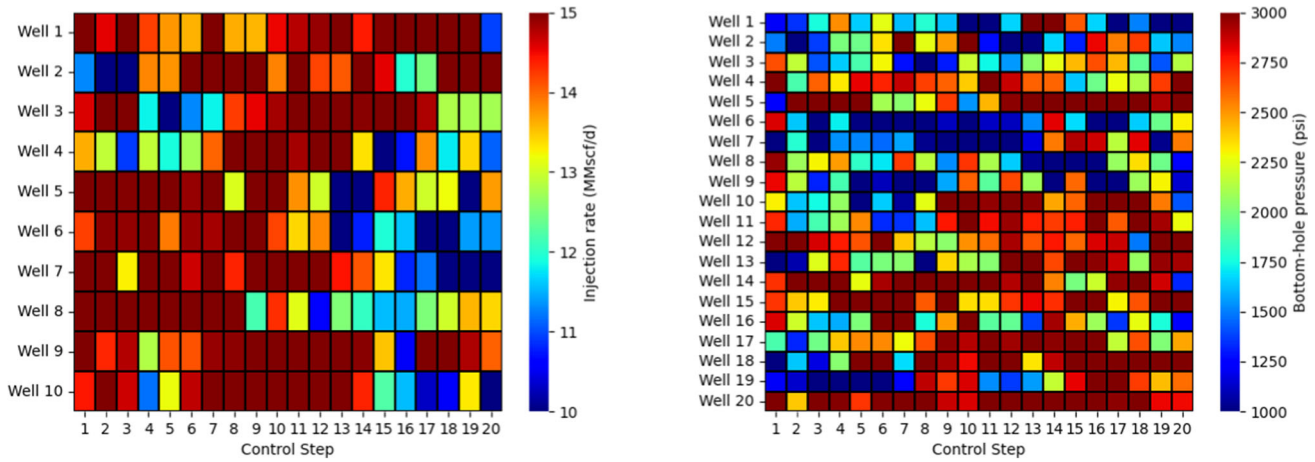

(a) Injection **(b)** Production

Fig. 7 Optimal well control schedules for the bi-objective optimization problem. (a) Injection rates for 10 wells and (b) Bottom-hole pressures for 20 producers

Another important remark is that, although in this specific example, the NPCTC is much lower than the NPV in terms of monetary value, it does not directly translate to a lower order of importance. For the energy industry, the carbon credit itself also represents the capability of one to compensate for their greenhouse emission. The real market of carbon credits is very complex, so focusing on it is not the scope of our study, but we convey our point of NPCTC being much more important than its monetary value.

The heatmaps at the bi-objective optimum shown in Fig. 7 differ from the ones in Fig. 4, especially the injection rates to maximize the amount of CO_2 storage, contributing directly to the negative NPCTC objective function. Figure 8 shows the values of enforced nonlinear state constraints onto the optimization problem. Again, the LS-SQP algorithm honors these constraints accurately with no violation at the bi-objective optimum. This result is also consistent with the observations in Fig. 5, as the maximum values of FLPR and FWPR occur at the same control time steps as of the single-objective optimum.

Figure 9 compares the trapped (or sequestered) CO_2 saturation distributions after 3600-day life-cycle simulation for the uniform midpoint initialization, the single-objective NPV optimum, and the bi-objective optimum with $\gamma = 0.99$, respectively. We observe that at the bi-objective optimum, the amount of CO_2 trapped increases quite significantly compared to the one at the single-objective optimum.

We also construct the approximation of the Pareto front by repeatedly solving the bi-objective optimization problem with different values of γ. Lower values of γ means more relaxation on the NPV constraint, resulting in a larger feasible region for the objective function $J_{\text{NPCTC}}(\bar{\mathbf{u}})$ to further decrease. Figure 10 shows the numerical construction of the Pareto front for $\gamma = \{0.7, 0.75, 0.8, 0.85, 0.9, 0.95, 0.99\}$. Note that on for each datapoint generated, the optimal NPV value found does not necessarily have to be close (or even

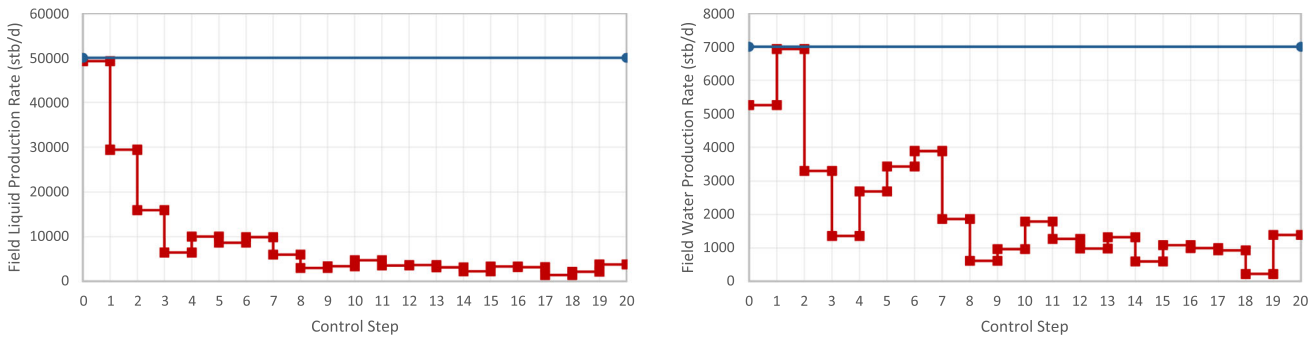

(a) Field liquid production rate (FLPR) **(b)** Field water production rate (FWPR)

Fig. 8 Enforced nonlinear constraint values at the optimum of the bi-objective problem. (a) Field liquid production rate vs. control steps and (b) Field water production rate vs. control steps

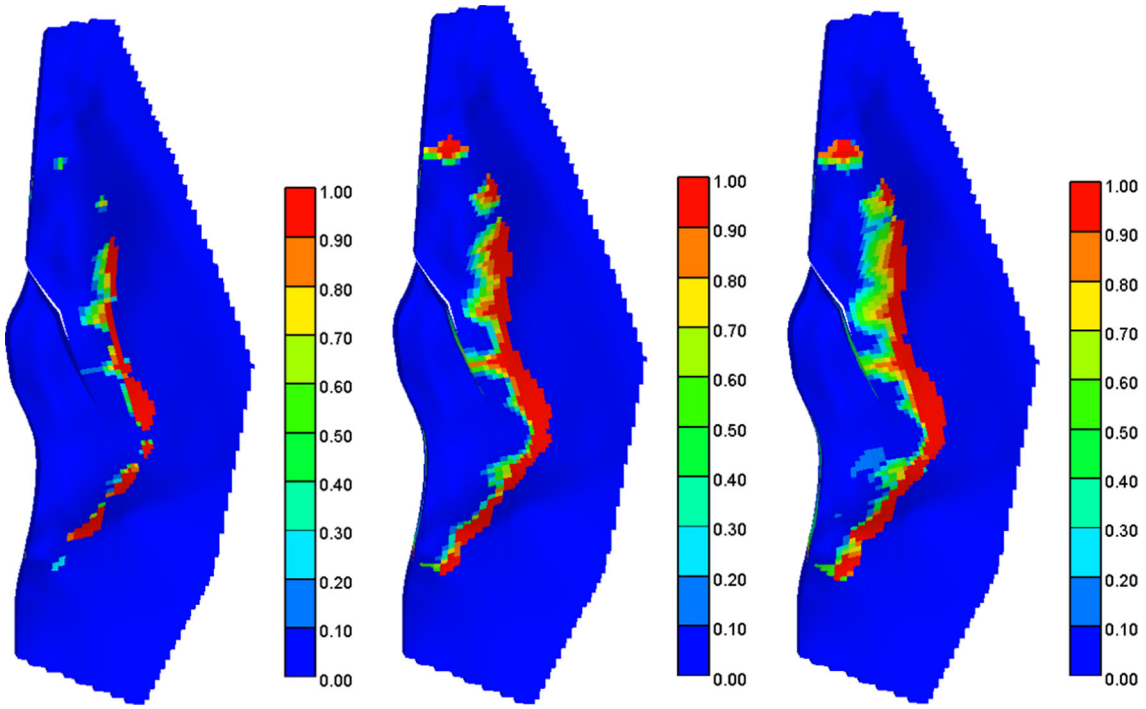

(a) Unoptimized (Initialization) **(b)** Single-objective optimum **(c)** Bi-objective optimum $\gamma = 0.99$

Fig. 9 Top-view comparison of the trapped CO_2 saturation distributions after life-cycle simulation: (a) Initial distribution of CO_2 concentration, (b) Distribution of CO_2 concentration after single-objective optimization, and (c) Distribution of CO_2 concentration after bi-objective optimization with $\gamma = 0.99$. Color bars in the figures represent CO_2 concentration in fraction

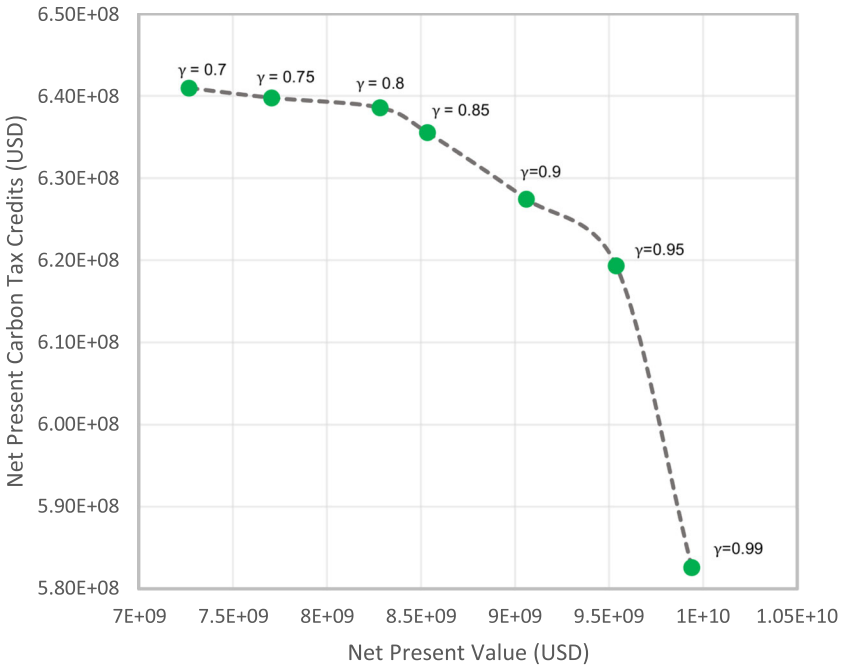

Fig. 10 Numerical approximation of the Pareto front of the bi-objective optimization problem

equal) to the bound value $\left|\gamma J_{\mathrm{NPV}}(\bar{\mathbf{u}}^*)\right|$ as specified in the constraint Eq. 12b. We also observe that there is no significant improvement on the value of NPCTC for $\gamma \leq 0.8$.

5 Summary and conclusions

In this paper, we extend and apply the LS-SQP workflow [34] to efficiently handle the production optimization problem as part of the CO_2-EOR design process on the Brugge model. A compositional fluid description is used for flow simulations performed within the context of optimization work. In the optimization procedure, we utilize the lexicographic method of solving the bi-objective optimization problem in order to achieve both the maximum NPV and NPCTC. The conclusions of this study can be stated as follows:

- The LS-SQP workflow solves the nonlinearly constrained single-objective optimization problem to find the maximum NPV of 10.04×10^9 USD. The corresponding NPCTC value is 5.12×10^8 USD.
- Using the lexicographic method, the LS-SQP workflow also efficiently solves the nonlinearly constrained bi-objective optimization problem. By allowing the maximum of 1% decrease ($\gamma = 0.99$) in the maximum NPV from the single-objective problem, the algorithm found an optimal NPCTC of 5.826×10^8 USD, resulting in a 13.8% uplift in the NPCTC compared to its value at the single-objective optimum. It is important to note that, depending on CCUS practitioners' priorities, the carbon credit can be more important than its mere monetary value.
- A numerical approximation of the Pareto front is constructed by varying the values of γ in the bi-objective optimization problem. Results showed that there is no significant increase in NPCTC for $\gamma \leq 0.8$ for the investigated compositional Brugge model.

6 Future work

We would like to extend our work here to robust optimization where multiple realizations are considered due to geological uncertainty, such as the Brugge case with 104 realizations or larger datasets like in [14]. The optimization procedures with different constraint handling methods presented in [34] could be useful in maintaining accuracy and efficiency due to an increasing number of constraints from uncertainty.

Acknowledgements The support of the member companies of Tulsa University Petroleum Reservoir Exploitation Projects (TUPREP) is gratefully acknowledged. The authors acknowledge the Computer Modeling Group (CMG) for making available multiple GEM licenses.

Declarations

Conflicts of interest The authors have no conflicts of interest to declare.

Appendix: supplemental data

Table 4 Compositional fluid data for Peng-Robinson EOS

Component	Molar Fraction	Critical Pressure (atm)	Critical Temperature (K)	Critical Volume (L/mol)	Molar Weight (g/gmol)	Acentric Factor	Parachor Coefficient
CO_2	0.0001	72.80	304.20	0.0940	44.01	0.2250	78.0
N_2-C_1	0.2203	45.24	189.67	0.0989	16.21	0.0084	76.5
C_1-C_4	0.2063	43.49	412.47	0.2039	44.79	0.1481	150.5
C_5-C_7	0.1170	37.69	556.92	0.3324	83.46	0.2486	248.5
C_8-C_{12}	0.2815	31.04	667.52	0.4559	120.52	0.3279	344.9
C_{13}-C_{19}	0.0940	19.29	673.76	0.7649	220.34	0.5672	570.1
C_{20}-C_{30}	0.0808	15.38	792.40	1.2521	321.52	0.9422	905.7

Table 5 Binary interaction parameters for the compositional fluid

Component	CO_2	N_2-C_1	C_1-C_4	C_5-C_7	C_8-C_{12}	C_{13}-C_{19}	C_{20}-C_{30}
CO_2	0	0.1013	0.1317	0.1421	0.1501	0.1502	0.1503
N_2-C_1	0.1013	0	0.0130	0.0358	0.0561	0.0976	0.1449
C_1-C_4	0.1317	0.0130	0	0.0059	0.0160	0.0424	0.0779
C_5-C_7	0.1421	0.0358	0.0059	0	0.0025	0.0172	0.0427
C_8-C_{12}	0.1501	0.0561	0.0160	0.0025	0	0.0067	0.0251
C_{13}-C_{19}	0.1502	0.0976	0.0424	0.0172	0.0067	0	0.0061
C_{20}-C_{30}	0.1503	0.1449	0.0779	0.0427	0.0251	0.0061	0

Table 6 Summary of the LS-SQP optimization parameters

LS-SQP Parameter	**Notation**	**Value**
Maximum number of gradient recomputations	$n_{\text{grad,max}}$	3
Maximum number of backtracking cuts	$n_{\text{cuts,max}}$	5
Maximum backtracking step size	α	1
Backtracking step size cut factor	ρ	0.5
Maximum number of optimization iterations	N_{iter}	200
Maximum objective function change tolerance	ϵ_{J}	10^{-3}
Maximum design vector change tolerance	ϵ_{u}	10^{-3}
StoSAG number of perturbations	N_{p}	10
StoSAG variance	σ^2	0.01^2
StoSAG temporal length of correlation	L	5

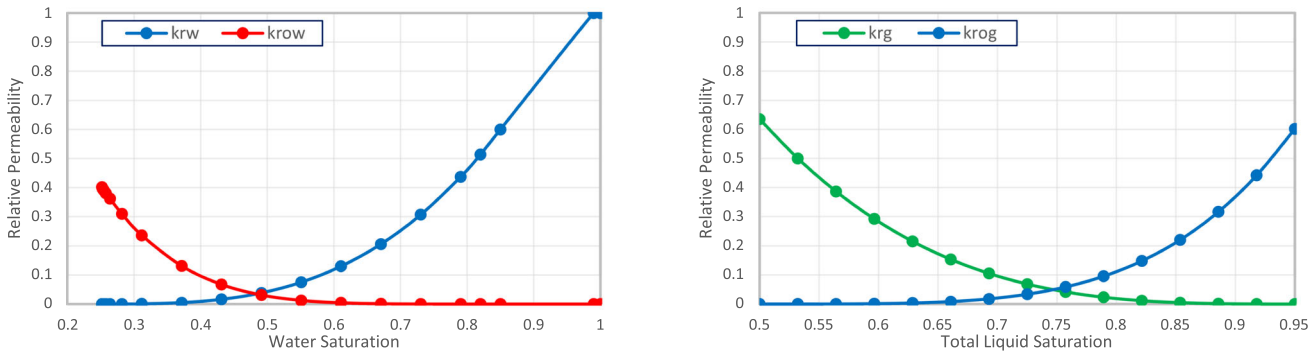

(a) Water-oil **(b)** Gas-liquid

Fig. 11 Relative permeability data: (a) Water-oil and (b) Gas-liquid

References

1. Almasov, A., Nguyen, Q., Onur, M.: Nonlinearly constrained life-cycle production optimization with a least-squares support-vector regression proxy. EAGE ECMOR **2022**(2022), 1–29 (2022)
2. Alpak, F., Jain, V., Wang, Y., Gao, G.: Biobjective Optimization of Well Placement: Algorithm, Validation, and Field Testing. SPE Journal **27**, 246–273 (2022)
3. Alpak, F. O., & Jain, V. (2022). An Accelerated Subsurface Field-Development Optimization Platform for the Geological Sequestration of CO2. 29-31 March 2022 of *AAPG Carbon Capture, Utilization, and Storage Conference*. AAPG
4. Antoniou, A., & Lu, W. (2007). *Practical optimization: algorithms and engineering applications*. Springer Science & Business Media
5. Atadeger, A., Onur, M., Sheth, S., & Banerjee, R. (2023). Deep Learning-Based and Kernel-Based Proxy Models for Nonlinearly Constrained Life-Cycle Production Optimization. Day 2 Wed, January 25, 2023 of *SPE Reservoir Characterisation and Simulation Conference and Exhibition*. SPE-212690-MS
6. Bonyadi, M.R., Michalewicz, Z.: Particle Swarm Optimization for Single Objective Continuous Space Problems: A Review. Evolutionary Computation **25**, 1–54 (2017)
7. Brouwer, D. R., Nævdal, G., Jansen, J. D., Vefring, E. H., & van Kruijsdijk, C. P. J. W. (2004). Improved reservoir management through optimal control and continuous model updating. In *Proceedings of the SPE Annual Technical Conference and Exhibition, Houston, Texas, 26-29 September* SPE 90149
8. Chen, B., Fonseca, R.-M., Leeuwenburgh, O., Reynolds, A.C.: Minimizing the risk in the robust life-cycle production optimization using stochastic simplex approximate gradient. Journal of Petroleum Science and Engineering **153**, 331–344 (2017)

9. Chen, B., Reynolds, A.C.: Co2 water-alternating-gas injection for enhanced oil recovery: Optimal well controls and half-cycle lengths. Computers & Chemical Engineering **113**, 44–56 (2018)
10. Chen, B., Reynolds, A.C., et al.: Ensemble-based optimization of the water-alternating-gas-injection process. SPE Journal **21**, 786–798 (2016)
11. Chen, C., Li, G., Reynolds, A.C.: Closed-loop reservoir management on the Brugge test case. Computational Geosciences **14**, 691–703 (2010)
12. Chen, C., Li, G., & Reynolds, A. C. (2011). Robust Constrained Optimization of Short and Long-Term NPV for Closed-Loop Reservoir Management. All Days of *SPE Reservoir Simulation Conference*. SPE-141314-MS
13. Chen, Y., Oliver, D.: Ensemble-based closed-loop optimization applied to Brugge field. SPE Reservoir Evaluation & Engineering **13**, 56–71 (2010)
14. Cremon, M.A., Christie, M.A., Gerritsen, M.G.: Monte carlo simulation for uncertainty quantification in reservoir simulation: A convergence study. Journal of Petroleum Science and Engineering **190**, 107094 (2020)
15. Das, I., Dennis, J.E.: Normal-boundary intersection: A new method for generating the pareto surface in nonlinear multicriteria optimization problems. SIAM Journal on Optimization **8**, 631–657 (1998)
16. Dehdari, V., Oliver, D.S.: Sequential quadratic programming for solving constrained production optimization-case study from Brugge field. SPE Journal **17**, 874–884 (2012)
17. Do, S., Reynolds, A.C.: Theoretical connections between optimization algorithms based on an approximate gradient. Computational Geosciences **17**, 959–973 (2013)
18. Fonseca, R. R. M., Chen, B., Jansen, J. D., & Reynolds, A. (2016). A stochastic simplex approximate gradient (StoSAG) for optimization under uncertainty. *International Journal for Numerical Methods in Engineering*,
19. Gass, S., Saaty, T.: The computational algorithm for the parametric objective function. Naval Research Logistics Quarterly **2**, 39–45 (1955)
20. Gen, M., Cheng, R.: Genetic algorithms and engineering optimization, vol. 7. John Wiley & Sons (2000)
21. Isebor, O.J., Durlofsky, L.J.: Biobjective optimization for general oil field development. Journal of Petroleum Science and Engineering **119**, 123–138 (2014)
22. Jansen, J., Brouwer, D., Naevdal, G., van Kruijsdijk, C.: Closed-loop reservoir management. First Break **23**, 43–48 (2005)
23. Jones, A. C., & Sherlock, M. F. (2021). *The Tax Credit for Carbon Sequestration (Section 45Q)*. Congressional Research Service Research Report Congressional Research Service
24. Kraaijevanger, J. F. B. M., Egberts, P. J. P., Valstar, J. R., & Buurman, H. W. (2007). Optimal waterflood design using the adjoint method. In *Proceedings of the SPE Reservoir Simulation Symposium* SPE 105764 (p. 15)
25. Li, Y., Nguyen, Q., & Onur, M. (2022). Physics-Based Data-Driven Interwell Simulator for Waterflooding Optimization Considering Nonlinear Constraints. Day 4 Thu, June 09, 2022 of *SPE Europec featured at EAGE Conference and Exhibition*. SPE-209634-MS
26. Liu, X., Reynolds, A.C.: Augmented Lagrangian Method for Maximizing Expectation and Minimizing Risk for Optimal Well-Control Problems With Nonlinear Constraints. SPE Journal **21**, 1830–1842 (2016)
27. Liu, X., Reynolds, A.C.: Gradient-Based Multiobjective Optimization for Maximizing Expectation and Minimizing Uncertainty or Risk With Application to Optimal Well-Control Problem With Only Bound Constraints. SPE Journal **21**, 1813–1829 (2016)
28. Liu, Z., Forouzanfar, F., Zhao, Y.: Comparison of SQP and al algorithms for deterministic constrained production optimization of hydrocarbon reservoirs. Journal of Petroleum Science and Engineering **171**, 542–557 (2018)
29. Liu, Z., Reynolds, A.: Robust Multiobjective Nonlinear Constrained Optimization with Ensemble Stochastic Gradient Sequential Quadratic Programming-Filter Algorithm. SPE Journal **26**, 1964–1979 (2021)
30. Liu, Z., & Reynolds, A. C. (2019). An sqp-filter algorithm with an improved stochastic gradient for robust life-cycle optimization problems with nonlinear constraints. In *SPE Reservoir Simulation Conference*. Society of Petroleum Engineers
31. Lu, R., Forouzanfar, F., & Reynolds, A. C. (2017). Bi-Objective Optimization of Well Placement and Controls Using StoSAG. Day 1 Mon, February 20, 2017 of *SPE Reservoir Simulation Conference*. SPE-182705-MS
32. Marler, R.T., Arora, J.S.: Survey of multi-objective optimization methods for engineering. Structural and multidisciplinary optimization **26**, 369–395 (2004)
33. Moore, E.H.: On the Reciprocal of the General Algebraic Matrix. Bulletin of the American Mathematical Society **26**, 385–396 (1920)
34. Nguyen, Q. M., Onur, M., & Alpak, F. O. (2023). Nonlinearly Constrained Life-Cycle Production Optimization Using Sequential Quadratic Programming (SQP) With Stochastic Simplex Approximated Gradients (StoSAG). All Days of *SPE Reservoir Simulation Conference*. SPE-212178-MS
35. Nocedal, J., Wright, S.J.: Numerical Optimization. Springer, New York (2006)
36. Penrose, R.: A generalized inverse for matrices. Mathematical Proceedings of the Cambridge Philosophical Society **51**, 406–413 (1955)
37. Peters, L., Arts, R., Brouwer, G., Geel, C., Cullick, S., Lorentzen, R., Chen, Y., Dunlop, K., Vossepoel, F., Xu, R., Sarma, P., Alhuthali, A., Reynolds, A.: Results of the Brugge benchmark study for flooding optimisation and history matching. SPE Reservoir Evaluation & Engineering **13**, 391–405 (2010)
38. Schmelz, W.J., Hochman, G., Miller, K.G.: Total cost of carbon capture and storage implemented at a regional scale: northeastern and midwestern united states. Interface Focus **10**, 20190065 (2020)
39. Smith, E., Morris, J., Kheshgi, H., Teletzke, G., Herzog, H., Paltsev, S.: The cost of co2 transport and storage in global integrated assessment modeling. International Journal of Greenhouse Gas Control **109**, 103367 (2021)
40. Sun, Z., Xu, J., Espinoza, D. N., & Balhoff, M. T. (2021). Optimization of subsurface co2 injection based on neural network surrogate modeling. *Computational Geosciences*, *25*
41. Wang, Y., Alpak, F., Gao, G., Chen, C., Vink, J., Wells, T., Saaf, F.: An Efficient Bi-Objective Optimization Workflow Using the Distributed Quasi-Newton Method and Its Application to Well-Location Optimization. SPE Journal **27**, 364–380 (2022)
42. Yu, W., Lashgari, H., & Sepehrnoori, K. (2014). Simulation Study of CO2 Huff-n-Puff Process in Bakken Tight Oil Reservoirs. All Days of *SPE Western Regional Meeting*. SPE-169575-MS
43. Zadeh, L.: Optimality and non-scalar-valued performance criteria. IEEE Transactions on Automatic Control **8**, 59–60 (1963)